Available Online

JOURNAL OF SCIENTIFIC RESEARCH

J. Sci. Res. **14** (2), 545-558 (2022)

www.banglajol.info/index.php/JSR

Synthesis, X-ray Crystallography, Hirshfeld Surface Analysis, Spectral Analysis, and Molecular Docking Studies on (E)–2–(1–(4–Fluorophenyl)Ethylidene) Hydrazine Carbothioamide

M. Sivasubramanian[1*], R. R. Saravanan[2], R. Mendoza-Meroñob[3]

[1]Department of Physics, Government Arts College (Autonomous), Kumbakonam, India–612002 (Affiliated to Bharathidasan University, Tiruchirappalli)

[2]Department of Physics, Meenakshi Chandrasekaran College of Arts and Science, Pattukkottai, Thanjavur, Tamil Nadu, India– 614626 (Affiliated to Bharathidasan University, Tiruchirappalli)

[3]Department of Physical and Analytical Chemistry, University Oviedo, C/ Julian Claveria, 8, 33006, Oviedo (Asturias), Spain

Received 22 December 2021, accepted in final revised form 11 March 2022

Abstract

Synthesis, X-ray crystallography, spectral analysis, and molecular docking analysis on (E)–2–(1–(4–fluorophenyl) ethylidene) hydrazine carbothioamide (EFEHC) are performed. Thiosemicarbazones are a class of small molecules used as anticancer therapeutics. The FT–IR and FT-Raman spectra of EFEHC have been recorded in 4000–400 and 4000–100 cm^{-1}, respectively. The present communication deals with the quantum chemical calculations of energies, geometrical structure, and vibrational wavenumbers of EFEHC using the density functional (DFT/B3LYP) method with 6–31G (d, p) basis set. The conformational analysis gives the energy values based on the change in the position of atoms in the EFEHC molecule. Hirshfeld surface analysis (HSs) is used to discuss the evaluation of intermolecular interactions. Molecular docking analysis of the small molecule EFEHC with macromolecule HMG–CoA protein showed that this is a good molecule and is suitable for anti-cholesterol targets.

Keywords: Molecular structure; Hirshfeld surface analysis; Crystal growth; DFT; Molecular docking; FT-IR; FT-Raman.

doi: http://dx.doi.org/10.3329/jsr.v14i2.57111 J. Sci. Res. **14** (2), 545-558 (2022)

1. Introduction

Semicarbazones and related compounds have a consistent role in designing novel anticonvulsant agents [1]. A number of semicarbazones, thiosemicarbazones [2], bis carbo hydrazones, aryl, arylidene, aryloxy aryl semicarbazones, acetyl hydrazones, and oxazolyl hydrazones are synthesized and evaluated for anticonvulsant activity [3]. Moreover, several pyridine ring-containing compounds are known for their varied biological activities like antibacterial, antitubercular, antihistaminic effects.

* *Corresponding author*: uitunna@gmail.com

Thiosemicarbazides are versatile ligands having p-delocalization of charge and configurational flexibility of the molecular chain that can give rise to a great variety of coordination modes owing to the interest they generate through a variety of biological properties ranging from anticancer, antitumor, antifungal antibacterial, antimalarial, anti filarial, antiviral and anti-HIV activities [4]. Following this report, various aliphatic, aromatic, and heteroaromatic carbaldehyde thiosemicarbazones were synthesized and evaluated for antitumor activity against a wide spectrum of transplanted murine neoplasms [5].

Synthesis, X-ray crystallography, DFT calculations, molecular geometry, conformational stability, vibrational spectroscopic analysis, and Hirshfeld Surface analysis have been performed. The Molecular docking studies of EFEHC crystal show that it is suitable for the Cholesterol target. In docking, EFEHC interacts with the 1DQ8 protein target, and it gives a negative energy value with a hydrogen bond.

2. Experimental

2.1. *Sample preparation*

The 1–(4–Fluorophenyl)ethanone and thiosemicarbazide compounds in the solid-state with ≥98.0 % purity (Merck GR) were used for the synthesis of EFEHC material. The solution of 1–(4–Fluorophenyl)ethanone (2.76 g 0.02 Mol) and thiosemicarbazide (1.82 g, 0.02 Mol) were taken with the absolute methanol (80 mL) in a round bottom flask. It was refluxed for 2 h in the presence of a p–toluenesulfonic acid as a catalyst, with continuous stirring. The Teflon platform stirs the internal solution at a speed of 150 rpm to 300 rpm. On cooling to room temperature, the precipitate was filtered off. The resulting product was collected, washed with copious cold methanol, dried, and recrystallized using methanol.

2.2. Computation details for density functional theory calculations

The entire calculations were performed at B3LYP levels that are included in the Gaussian 09W [6] package with the 6–31G (d, p) basis set functions of the DFT utilizing gradient geometry optimization [7] employing Becke's three-parameter hybrid functional [8] combined with the Lee-Yang–Parr correlation [9] functional (B3LYP) method for obtaining the geometry optimization as it is moderate and suitable for such organic molecular structures [10]. The energy calculations were carried out for four different possible conformers.

3. Results and Discussion

3.1. *Molecular structure analysis*

The EFEHC crystal structure belongs to a triclinic system with P–1 symmetry. The molecule shows the thione form and E–configuration of hydrazine bonds in the crystal state. The bond length N(1)–N(2) (1.385 (2) Å) and the dihedral angle C(7)═N(1)N(2)–C(9)(170.97(2)°) are similar to those found for thiosemicarbazone systems in CSD [11] (selected 371 hits, average distance N–N is 1.374 Å and mean dihedral angle is 178.21°). The dihedral angle between the principal structural moieties, the fluorobenzene ring C1/C2/C3/C4/C5/C6/F1 (C3 atom max. deviation = 0.0112 (2) Å) and the moiety C7/N1/N2/C9/S1/N3 (N1 atom max. deviation = 0.1127 (2) Å) is 48.24 (1)° [12] in which the F atom is in the ortho position, i.e., 55.77 (1)°.

Table 1. Crystal Data and Structure Refinement for EFEHC.

Formula	C9 H10 F N3 S
Formula weight (g mol–1)	211.26
Temperature (K)	293(2)
Wavelength	MoK\a (0.71073 Å)
Crystal system	Triclinic
Space group	P–1
Unit cell dimensions	
a (Å)	8.3300(7)
b (Å)	8.6610(8)
c (Å)	9.0750(8)
α (°)	74.680(5)
β(°)	65.580(4)
γ (°)	61.370(4)
Cell volume ($Å^3$)	521.47(8)
Z	2
Calc. Density (mg m^{-3})	1.345
Absorption coefficient (mm^{-1})	0.288
F(000)	220
Crystal size (mm^3)	0.20 x 0.20 x 0.20
Theta range for data collection (°)	2.5 – 27.5
Index ranges	$-10 \leq h \leq 10$, $-11 \leq k \leq 11$, $-11 \leq l \leq 11$
Reflections collected	5397
Independent reflections	1968 (R_{int} = 0.0361)
Completeness (%)	99.91
Data/restraints/parameters	2363/0/139
Goodness–of–fit on F^2	1.084
Final R indices ($I>2\sigma(I)$)	R1 = 0.0454 wR2 = 0.1358
R indices (all data)	R1 = 0.0530 wR2 = 0.1415
Largest diff. peak and hole	0.346 and –0.327 e $Å^{-3}$

In the crystal packing, the molecules are linked into two–dimensional layers by intermolecular N—H···S hydrogen–bond interactions, which generate chains. These chains are formed by two types of centrosymmetric synthon (I and II) through the amine

and thioamide hydrogens. On the other hand, the strong N–H···F hydrogen bond connects the fluorobenzene rings with the chain-smoking (green), providing additional crystal stability. Additionally, π–π stacking interactions (Cg1(C1 → C6)···Cg1(iv) = 4.4254(2) Å, offset = 36.67° for iv: 1–x,1–y,–z) are present in the crystal and are well orientated, which are contributing to stabilizing chains. Tables 1 and 2 describe the crystallographic data and hydrogen geometry. The ORTEP diagram and crystal packing of EFEHC are shown in Figs. 1 and 2, respectively.

Table 2. Hydrogen-bond geometry (Å, º).

D—H•••A	D—H (Å)	H•••A (Å)	D•••A (Å)	D—H•••A (º)
N(2)—H(9)•••S(1) (i)	0.89(3)	2.69(3)	3.577(2)	179.0(2)
N(3)—H(10a)•••N(1) (ii)	0.83(3)	2.21(2)	2.598(2)	107.0(2)
N(3)—H(10a)•••F(1) (iii)	0.85(2)	2.27(2)	3.045(2)	150.(2)
N(3)—H(10b)•••S(1) (iv)	0.91(3)	2.59(3)	3.4735(2)	165.0(3)

Symmetry Codes (i) –1–x, 2–y, 1–z (ii)–x, y, z (iii) 1–x,2–y,–z (iv)–1–x,3–y,1–z

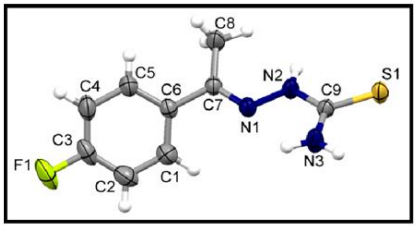

Fig. 1. ORTEP diagram of EFEHC.

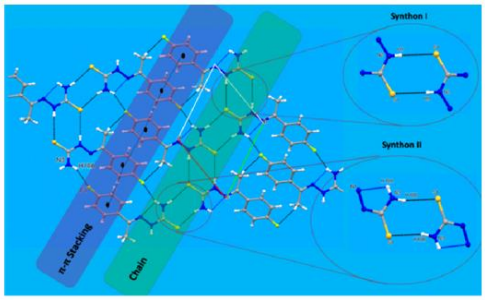

Fig. 2. Crystal packing of EFEHC.

3.2. *Conformational analysis*

In order to find the most optimized geometry, the energy calculations were carried out for EFEHC. The different conformers of EFEHC molecule are shown in Fig. 3. Conformational energy values for all the four conformers of EFEHC are presented in Table 3. In the structure of EFEHC, conformer C4 is the most stable conformer with energy –2654957.803 KJ/Mol. The conformer C2 is the low stable conformer with energy –2654767.705 KJ/Mol. The Zero points corrected optimized energy of the conformers is predicted at –1011.21980615 AU (C4), –1011.19963558 AU (C3), –1011.16020515 AU (C1), and –1011.14740155 AU (C2). The relative energy of the conformers is determined at 0.0 kJ/Mol (C4), 52.95 kJ/Mol (C3), 156.36 kJ/Mol (C1), and 190.09 kJ/Mol (C2) for B3LYP/6–31G(d,p) level of theory.

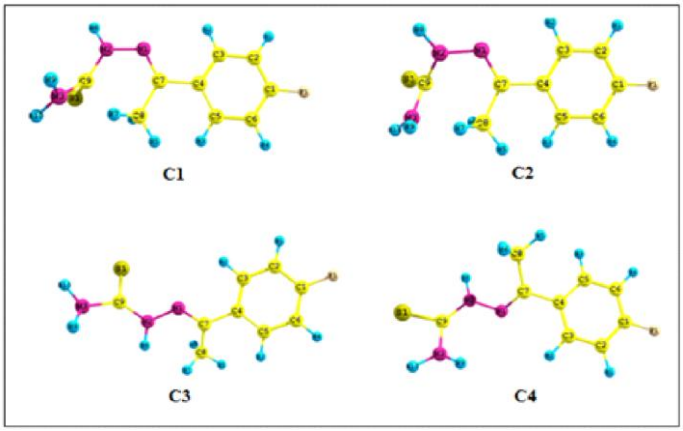

Fig. 3. Conformers of EFEHC.

Table 3. Total Energies of Different Conformations of EFEHC Calculated at the B3LYP/ 6–31G (d, p) Level of Theory.

Code	Energy (Hartree)	KJ/Mol	Energy Difference (KJ/Mol)
C4	–1011.219806	–2654957.803	0
C3	–1011.199636	–2654904.845	52.95783557
C1	–1011.160205	–2654801.443	156.3607455
C2	–1011.147402	–2654767.705	190.0982918

3.3. *Molecular electrostatic potential analysis*

MEP analysis plays an important role in analyzing the molecular structure of its physicochemical property relationships [13]. Molecular electrostatic potential surfaces are important in computer-aided drug design because they assist in the optimization of electrostatic interactions between the protein and the legend. To predict reactive sites for an electron acceptance and electron contribution attack on the EFEHC molecule, MEP was calculated at the B3LYP/6–31G (d,p) level basis set. The red color or negative regions of MEP were related to electrophilic reactivity, and the blue color or positive regions were related to. It is nucleophilic reactivity shown in Fig. 4. The molecular electrostatic potential (MEP) is related to the electronic density. It is a very useful descriptor for determining sites for electrophilic attack and nucleophilic reactions and hydrogen–bonding interactions [14]. The EFEHC molecule must present atoms either with positive potential isosurface or with negative potential isosurface. The MEP of EFEHC clearly indicates the electron-rich centers of sulfur and the positive potential isosurface centers of N1 & H9.

Table 4. Theoretical and experimental vibrational wavenumbers (cm^{-1}) of EFEHC calculated by B3LYP/6–31G(d,p).

υ_{Raman} cm^{-1}	υ_{IR} cm^{-1}	υ_{cal} cm^{-1}	Reduced Mass	Force Const	IR Intensity	Raman Activity	Polarization ratio	Characterization of normal modes with PED (%)
–	–	38	10.129	0.0094	1.2867	2.6648	0.7430	τNNC(53)+τCCN(24)
–	–	43	3.8008	0.0044	0.1329	7.5276	0.6220	τCCC(67)+τCNN(20)
–	–	63	7.6768	0.0193	2.3381	1.3444	0.6856	βCCN(22)+βCNN(22)
–	–	98	3.6358	0.0221	0.6188	4.9736	0.4491	τCNN(53)+τCCC(20)
109	–	109	5.2174	0.0395	1.6083	0.6082	0.7476	τCCC(23)+τNNC(15)
136	–	135	1.4546	0.0170	0.7507	0.4940	0.7394	τHCC(61)
193	–	188	3.9673	0.0894	8.0503	1.3069	0.7135	βCCC(20)+βNCS(19)
220	–	225	5.1745	0.1667	8.6423	2.7367	0.4211	τCCF(16)+τCCN(12)
–	–	253	1.7131	0.0695	106.11	1.4212	0.7338	γNHC(49)
269	–	271	2.7442	0.1279	65.222	2.5216	0.4237	γNHC(27)+τCCC(17)
301	–	309	2.8152	0.1708	5.1375	1.6444	0.2941	βCCN(45)+βNCN(15)
369	–	364	7.1706	0.5992	20.441	2.5220	0.7330	βCCF(30)+βCCC(10)
375	–	377	7.2431	0.6536	13.669	1.8759	0.4286	τCCN(22)+τCCC(19)
–	–	403	4.3673	0.4518	0.9107	2.0513	0.2814	βNCC(21)+βCCF(17)+τCCC(15)
415	–	412	3.3288	0.3587	0.4717	4.4664	0.3673	τCCC(63)
432	–	438	3.9708	0.4844	4.7166	10.590	0.3375	βNCN(27)+βCCC(12)+βCCF(11)
477	–	470	1.2134	0.1704	93.006	2.1372	0.6417	τHNC(71)
490	–	495	2.9576	0.4606	24.481	1.3274	0.3505	τCCC(17)+τCCF(13)
531	–	532	4.4258	0.7974	5.7385	2.1449	0.1339	βCCN(17)+γSC(12)
556	–	558	2.9298	0.5805	0.2905	5.4917	0.5235	φCCN(41)+τCCC(10)
562	–	570	4.5595	0.9402	11.708	5.9987	0.4306	βCCC(14)+βCNN(12)
577	–	574	1.4911	0.3121	4.7889	0.4030	0.5541	τHNC(75)
–	628	623	3.2436	0.8014	0.5793	10.275	0.7285	γSNN(55)
625	–	626	4.1175	1.0263	0.4496	5.2325	0.7361	βCCC(21)
693	–	694	4.6204	1.4146	2.2142	2.9560	0.6916	τCCC(40)
714	713	699	3.9784	1.2361	8.4961	9.4340	0.4479	γCC(19)
793	–	798	1.2566	0.5088	2.7059	12.225	0.3491	τHCC(41)+τCCF(19)
814	813	811	4.9127	2.0556	43.841	11.585	0.1052	γCC(18)+γCC(17)+γFC(16)
822	–	818	1.6266	0.6920	46.285	2.0683	0.6292	τHCC(41)+τCCF(19)
836	833	833	3.0991	1.3657	34.093	43.731	0.1356	γSC(23)+βHNC(14)
913	–	917	1.2755	0.6809	0.1639	2.6485	0.7386	τCCC(49)+τCCF(29)
940	–	935	1.3151	0.7304	0.9108	3.2186	0.2674	γCCH(58)+τHCC(23)
970	971	957	3.0105	1.7525	20.054	0.6681	0.7498	γCC(33)+βHCC(16)
994	–	991	2.5426	1.5879	1.6484	0.3308	0.7495	βCCC(37)+βCCC(31)
–	–	1007	1.5899	1.0242	0.8891	23.842	0.3448	γCHC(66)+βHCH(11)
1013	1016	1015	2.0150	1.3198	18.685	28.856	0.4321	γNC(23)+βHNC(15)+γHCH(15)
1063	–	1067	2.3265	1.6824	22.952	114.80	0.2353	βCCC(12)+γCHC(10)
1088	1079	1087	1.4012	1.0511	25.278	4.7978	0.6707	βHCC(23)+βHCC(16)+γCC(14)
1112	–	1119	3.4488	2.7426	123.68	64.036	0.3315	γNN(59)
1158	1159	1144	1.1818	0.9821	20.884	78.277	0.2278	βHCC(28)+βHCC(17)+βHCC(14)
1220	1221	1228	3.3899	3.3054	90.600	8.9993	0.6941	γFC(46)+βHCC(14)+γCC(10)
1244	1241	1244	1.9198	1.8889	379.62	40.692	0.3604	βHNN(29)+βHNC(27)+νSC(67)

–	–	1274	1.3035	1.3449	3.0894	4.1617	0.5965	βHCC(31)+βHCC(19)+βHCC(16)
–	1286	1288	4.5708	4.8184	32.531	377.63	0.3088	νCC(64)
1302	1299	1298	9.7865	10.484	6.9024	107.66	0.3376	νCC(36)
1374	1375	1365	1.2904	1.5272	9.5433	6.2586	0.5456	βHCH(49)+βHCC(24)
1397	–	1396	2.9915	3.7021	11.744	23.224	0.4195	νCC(65)
1408	1403	1406	2.6131	3.2846	101.42	100.12	0.2945	νNC(72)+βHNH(23)
1433	1429	1435	1.2162	1.5923	170.17	14.500	0.5171	γCHC(27)+βHCH(24)
1453	1448	1451	1.1142	1.4911	86.655	16.848	0.5844	βHCH(67)+γCHC(11)
1468	–	1476	1.5983	2.2142	458.19	3.7670	0.1899	βHNN(32)+βHCH(11)+νNC(70)
1497	1500	1503	2.517	3.6167	16.729	321.22	0.3911	βHCC(13)+βCCC(12)+βHCC(12)
–	–	1561	1.6183	2.5059	235.64	162.72	0.3416	βHNH(63)+νNC(78)
–	1569	1570	6.665	10.443	23.087	438.50	0.3328	νCC(82)
1587	1594	1593	7.1397	11.512	7.1422	1897.1	0.3252	νNC(85)
1605	1608	1609	7.3111	12.028	78.083	94.370	0.3667	νNC(85)
2913	2910	2921	1.0429	5.6526	6.6021	115.40	0.0091	νCH(93)
2974	2978	2970	1.1006	6.1687	9.0814	47.426	0.7425	νCH(98)
3046	3045	3052	1.0951	6.4809	7.1631	41.286	0.5802	νCH(91)
3086	–	3086	1.0879	6.5811	8.4170	43.742	0.7378	νCH(96)
3096	–	3094	1.0886	6.6233	3.4154	87.273	0.4530	νCH(97)
–	–	3104	1.0947	6.7018	6.3024	163.48	0.265	νCH(98)
3109	–	3108	1.0947	6.7201	2.7287	118.49	0.1375	νCH(67)
3441	–	3443	1.0758	8.1052	31.895	189.05	0.2029	νNH(97)
3455	3458	3458	1.0471	7.9583	37.142	118.60	0.1242	νNH(98)
3611	3615	3616	1.1039	9.1711	105.84	56.861	0.6545	νNH(97)

Abbreviations: ν– stretching, β – Bending, τ– torsion, γ– out of the plane.

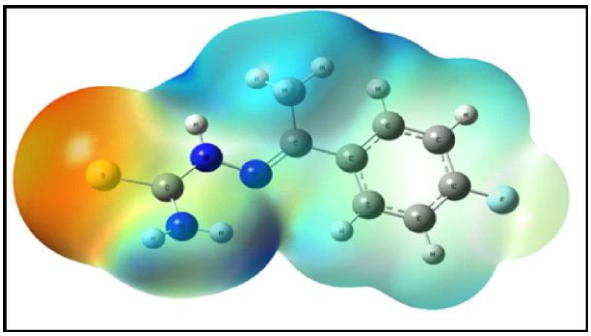

Fig. 4. Molecular electrostatic potential of EFEHC.

3.4. *Vibrational assignment*

The comparison of theoretical and experimental IR spectrum and Raman spectrum are shown in Figs. 5 and 6. Experimental and theoretical vibrational wavenumbers (cm^{-1}) calculated using B3LYP/6–31G (d,p) of EFEHC are shown in Table 4.

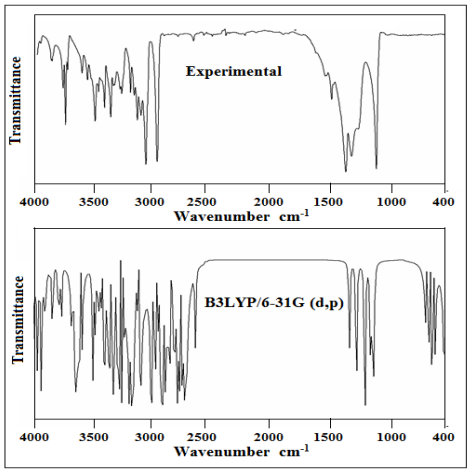

Fig. 5. FT–IR spectrum of EFEHC.

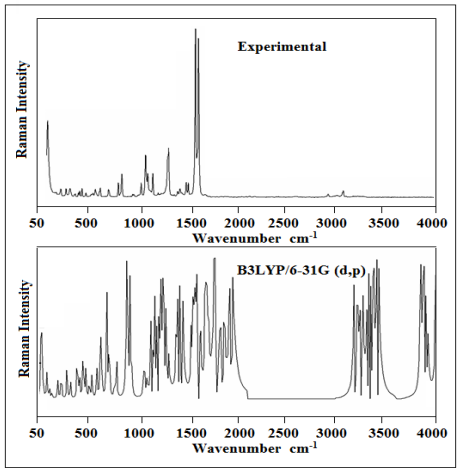

Fig. 6. FT–Raman spectrum of EFEHC.

3.5. *N–H vibrations*

In all the heterocyclic compounds, the Nitrogen–Hydrogen stretching vibrations take place in the region 3500cm^{-1} – 3300 cm^{-1} [15]. In the experimental FTIR spectrum of EFEHC observed at 3455 cm^{-1} and in FT–Raman, 3458 cm^{-1} is assigned to asymmetric N–H stretching vibration with PEDs 98%. The asymmetric stretching mode is calculated at 3458 cm^{-1} by B3LYP/6–31G (d,p).

3.6. *C–H vibrations*

The asymmetric C–H stretching mode of the CH_3 group is expected around 2980 cm$^{-1,}$ and the symmetric [16] one is expected in the region of 2870 cm^{-1}. The aromatic compounds normally exhibit many weak bands in the region 3100 cm^{-1}-2900 cm^{-1} due to aromatic C–H stretching vibrations. A weak band is observed at 3046, 2974 & 2913 cm^{-1} in the FT–IR spectrum, and an intense band is observed at 3045, 2978 & 2910 cm$^{-1,}$ and the FT–Raman spectrum can be assigned to C–H stretching respectively. The theoretically observed vibrations 3052, 2970, and 2920 cm^{-1} are calculated by B3LYP/6–31G (d,p) with PED 91, 98, and 93 %.

3.7. *C–C vibrations*

The Ring C–C stretching vibrations take place in the region of 1474–1666 cm^{-1} [16]. The frequencies observed for EFEHC in FT–IR spectrum at 1497 and 1587 cm^{-1} have been assigned to C–C stretching vibration. The corresponding vibrations appear in the FT–Raman spectrum at 1500 and 1594 cm^{-1}. The theoretically computed wavenumber at 1503 and 1593 cm^{-1} in the B3LYP method is also correlated with the experimental observations.

3.8. *C–F vibrations*

The assignments of C–F stretching modes are very difficult as these vibrations are strongly coupled with the other in-plane bending vibrations of several modes. Normally the observed bands of the C–F stretching vibrations have been found to be very strong in the FTIR spectra and these appear in the range between 1000–1300 cm^{-1} for several fluoros–benzenes [17].

The present molecule has one fluorine atom which is placed at the ortho position of the skeletal ring. In the present investigation, FTIR bands observed at 1220 cm^{-1} and the bands at 1221 cm^{-1} in the FT–Raman spectrum of EFEHC are assigned to the C–N stretching mode of vibrations. The calculated value at 1228 cm^{-1} is in excellent agreement with the experimental value for the corresponding vibration mode. The PED for C–F vibration is 46 %. According to the reported values [18], this assignment is in line with the literature.

3.9. *C–S vibrations*

C–S stretching bands are usually observed in the range of 670–930 cm^{-1} with moderate intensity. The calculated bands at B3LYP level in the same region show band positions at 832 cm^{-1} for the C–S stretching vibrations and are in excellent agreement with experimental observations of both FTIR and FT–Raman spectra.

4. HOMO-LUMO Analysis

FMOs have an impact on quantum chemistry. The values for HOMO and LUMO are -5.2192 eV and -7.4773 eV, respectively. The observed energy bandgap in the gas phase is 2.2580 eV. The ECHFPC HOMO-LUMO diagram is shown in Fig. 7. Essential characteristics such as global hardness (η), chemical potential (μ), and global electrophilicity index (ω) were calculated using ionization potential and electron affinity data. The results are 1.1290 eV, 6.3482 eV, and 17.8475 eV. Table 5 shows the EFEHC HOMO LUMO parameters. The occupied molecular orbital energies are all negative, confirming the structure's chemical stability.

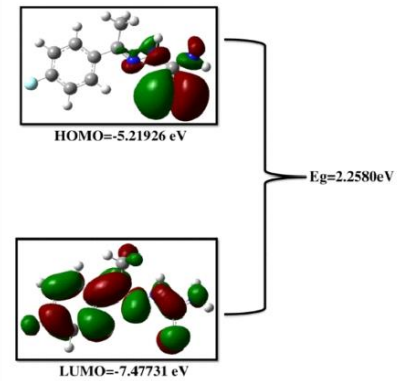

Table 5. Global parameters of EFEHC

HOMO energy	-5.21926 eV
LUMO energy	-7.47731 eV
Frontier molecular orbital energy gap	2.258052 eV
Global hardness(η)	1.129026 eV
Chemical potential(μ)	6.348287 Joule/kg)
Global Electrophilicity power(ω)	17.84758 (no dimension)

Fig. 7. HOMO LUMO analysis of EFEHC.

5. Thermodynamical Properties

Based on vibrational analysis at B3LYP/6-31G(d,p) levels, several thermodynamic parameters of EFEHC were theoretically calculated like zero-point vibrational energy, rotational constants, thermal energy, entropy, and enthalpy and was given in Table 6.

Table 6. Thermodynamic properties for EFEHC.

Parameters	Values B3LYP/6-31G(d,p)
Zero-point vibrational energy (kcal mol^{-1})	115.01892
Rotational Constants (GH_Z)	
A	1.40657
B	0.25098
C	0.21409
Thermal Energy (kcal mol^{-1})	
Total	123.563
Translation	0.889
Rotational	0.889
Vibrational	121.786
Entropy (cal mol^{-1} kelvin)	
Total	50.811
Translation	2.981
Rotational	2.981
Vibrational	44.849
Enthalpy (cal mol^{-1} kelvin)	
Total	118.869
Translation	41.945
Rotational	32.720

6. Molecular Docking Studies

The bioinformatics tools used in this study are Autodock tools (ADT) v1.5.4 and Autodock v4.2 program; (Autodock, Autogrid, Autotors, Copyright–1991e2000) from the

Scripps Research Institute, (http://www.scripps.edu/mb/ olson/doc/autodock), PyMOL 1.3, ChemDraw Ultra 11. The following compound (E)–2–(1–(4–fluorophenyl) ethylidene) hydrazine carbothioamide (EFEHC) were developed, and their three–dimensional structures were generated using ChemDraw Ultra, 11.0. The EFEHC molecule was structurally confirmed, and the energy was minimized using Gaussian 09W [6]. Three–dimensional structures of target protein HMG–CoA reductase (PDB ID: 1DQ8) were recovered from the Protein Data Bank (PDB) (http://www.pdb.org).

The probable binding sites of preferred target receptors were searched using Q–site Finder. The docking process was carried out using Auto dock tools [19] (ADT) v1.5.4 and Autodock v4.2 programs; (Autodock, Autogrid, Autotors, Copyright–1991e2000) from the Scripps Research Institute (http://www.scripps.edu/mb/olson/doc/autodock). Polar hydrogen charges of the Gasteiger–type were assigned, and the nonpolar hydrogens were merged with the carbons where the internal degrees of freedom and torsions were set. EFEHC were docked to target protein complexes HMG–CoA reductase (PDB ID: 1DQ8) with the molecules considered a rigid body and the ligand being flexible. The search was extended over the whole receptor protein used as blind docking. Affinity maps for all the atom types present and an electrostatic map were computed with a grid spacing of 0.375 Å. The search was carried out with the Lamarckian Genetic Algorithm; populations of 150 individuals with a mutation rate of 0.02 that evolved for 10 generations [20]. The evaluation of the results was done by sorting the different complexes with respect to the predicted binding energy. A cluster analysis based on the root mean square deviation values, with reference to the starting geometry, was subsequently performed. The lowest energy conformation of the most populated cluster was considered the most trustable solution.

Ligand–protein interactions of all the selected compounds were developed by the PyMol molecular viewer (The PyMOL Molecular Graphics System, Version 1.5.0.4 Schrödinger, LLC). The hydrophobic effect of ligands was developed by Pose view. This applet provides an interactive online prediction of protein-ligand interaction and environmental chemistry studies [21].

The hydrogen bonds between HMG–CoA, and EFEHC are also shown in Fig. 8. In docking, hydrogen bonding plays a significant role in interaction studies—hydrogen bonds formed between N1 and H9 in GLY808A and GLY766A with bond distances 3.2 and 2.2Å. The energy values between binding sites of HMG–CoA, and EFEHC are –3.54 kcal/Mol.

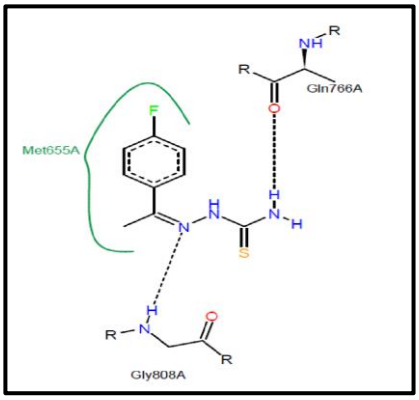

Fig. 8. Preview of EFEHC with HMG–CoA receptor.

7. Hirshfeld Surface Analysis

In order to explore a better understanding of intermolecular interactions to the supramolecular assembly, it is crucial to get quantitative measurements of these interactions. Hirshfeld Surface Analysis (HSA) [22] is becoming a valuable tool for elucidating molecular crystal structures quantitatively.

Hirshfeld Surfaces (HSs) and 2D fingerprint plots (FPs) were generated using Crystal Explorer 3.1 [23] based on the results of single-crystal X-ray diffraction studies. The function d_{norm} is a ratio encompassing the distances of any surface point to the nearest interior (d_i) and exterior (d_e) atom and the van der Waals radii of the atoms [24]. The molecular Hirshfeld Surface Analysis is a powerful technique for identifying the intermolecular short or long contacts within the crystal structure.

The Hirshfeld d_{norm} Surface, Shape Index, and Curvedness of the EFEHC molecule are shown in Fig. 9. The 2D fingerprint plots showing the percentage of area occupied by different intermolecular interactions are depicted in Fig. 10. The deep red circular spots indicate the short intermolecular contacts due to H…F hydrogen bonds. The sharp spikes in the fingerprint plot reveal the presence of H…F hydrogen bonds in the crystal structure of the EFEHC.

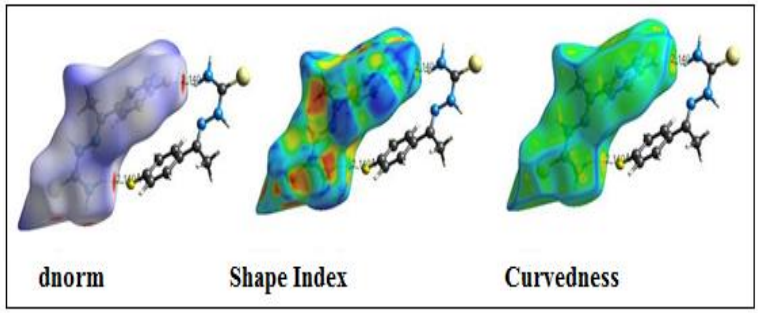

Fig. 9. Hirshfeld d_{norm} Surface, Shape Index and Curvedness of EFEHC

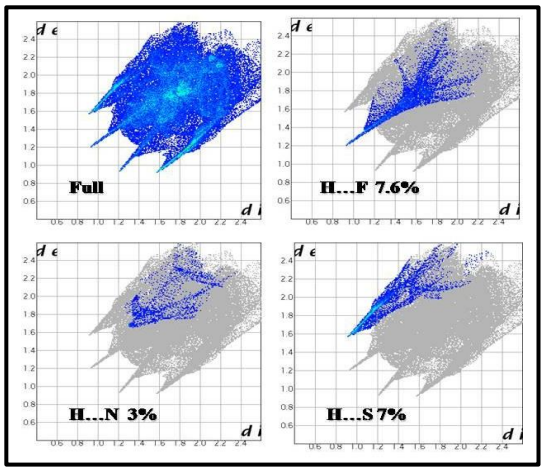

Fig. 10. Two–dimensional finger plot of EFEHC.

It shows the H…F hydrogen bonds with contact distance (d_e+d_i) = 2.140, comprising 7.6 % of the total Hirshfeld surface. Similarly, H…N covers 3%, and H…S covers 7 % of the total HSs.

5. Conclusion

In the present work, the geometry of the EFEHC was optimized with the DFT–B3LYP method using a 6–31G (d,p) basis set. The calculated structural parameters by the DFT method closely match with single crystal X-Ray diffraction data. Based on theoretically calculated total energy values, the C4 form is more stable than the other conformers. The presence of functional groups and their characteristics of EFEHC crystal have been identified by FT–IR, and FT–Raman spectral studies. Molecular electrostatic potential predicts the most reactive part of the molecule. The Hirshfeld Surface Analysis in decomposed fingerprint plots enables us to decode the intermolecular interaction types present in the EFEHC. The EFEHC ligand is suitable for the anti-cholesterol drug. The energy value between binding sites of HMG–CoA, and EFEHC is –3.54 kcal/Mol.

References

1. P. Yogeeswari, R. Thirumurugan, R. Kavya, S. Selwyn, P. S. James, and D. Sriram, Eur. J. Med. Chem. **39**, 729 (2004). https://doi.org/10.1016/j.ejmech.2004.03.008
2. S. N. Pandey, D. Sriram, G. Nath, and E. D. Clercq, Farmaco **54**, 624 (1999). https://doi.org/10.1016/S0014-827X(99)00075-0
3. Y. Perumal, S. Dharmarajan, and T. Rathinasabapathy, J. Med. Chem. **48**, 6202 (2005). https://doi.org/10.1021/jm050283b
4. S. N. Pandey, J. R. Dimmock, Pharmazie **48**, 659 (1993). https://doi.org/10.1136/thx.48.6.659
5. J. Easmon, G. Purstinger, G. Heinisch, T. Roth, H. H. Fiebig, et al., J. Med. Chem. **44**, 2164 (2001). https://doi.org/10.1021/jm000979z

6. M. J. Frisch, G. W. Trucks, H. B. Schlegel, G. E. Scuseria, M. A. Robb, et al., Gaussian-09, Revision A.01, Gaussian, Inc., Wallingford, CT, 2009.
7. H. B. Schlegel, J. Comput. Chem. **3**, 214 (1982). https://doi.org/10.1002/jcc.540030212
8. D. Becke, J. Chem. Phys. **108**, 9624 (1998). https://doi.org/10.1063/1.476438
9. C. Lee, W. Yang, R. G Parr, Phys. Rev. **B 37**, 785 (1988). https://doi.org/10.1103/PhysRevB.37.785
10. M. A. Kaloo1, H. Basheer, M. A. Rather, S. A. Majid, and B. A. Bhat, J. Sci. Res. **13**, 923 (2021). https://doi.org/10.3329/jsr.v13i3.50183
11. F. H. Allen, Acta Cryst. **B 58**, 380 (2002). https://doi.org/10.1107/S0108768102003890
12. J. G. Wang, F. F. Jian, J. Wang, and X. Liu, Acta Cryst. **E 63**, 608 (2007). https://doi.org/10.1107/S1600536806056480
13. T. Yesilkaynak, G. Binzet, F. Memen, U. Florke, N. Kulcu, et al., Eur. J. Chem. **1** (2010). https://doi.org/10.5155/eurjchem.1.1.1-5.3
14. N. Okulik and A. H. Jubert, Int. Electron. J. Mol. Des. **4**, 17 (2005).
15. D. Sajan, I. Hubert Joe, and V. S. Jayakumar, J. Raman Spectrosc. **37**, 508 (2005). ttps://doi.org/10.1002/jrs.1424
16. S. Yadav, A. Khare, K. Yadav, P. C. Maurya, A. K. Singh, et al., J. Sci. Res. **14**, 79 (2022). https://doi.org/10.3329/jsr.v14i1.53339
17. M. P. Kumpawat, A. Ojha, and N. D. Patel, Canad. J. Spectroscopy **25**, 1 (1980).
18. D. Mahadevan, S. Periandy, and S. Ramalingam, Spectrochimica Acta Part A **84**, 86 (2011). https://doi.org/10.1016/j.saa.2011.10.020
19. G. M. Morris, R. Huey, W. Lindstrom, M. F. Sanner, R. K. Belew, et al., J. Comput. Chem. **30**, 2785 (2009). https://doi.org/10.1002/jcc.21256
20. R. Huey, G. M. Morris, A. J. Olson, and D. S. Goodsell, J. Comput. Chem. **28**, 1145 (2007). https://doi.org/10.1002/jcc.20634
21. K. Stierand and M. Rarey, ACS Medicinal Chem. Lettt. **1**, 540 (2010). https://doi.org/10.1021/ml100164p
22. J. J. McKinnon, A. S. Mitchell, and M. A. Spackman, Chem. Eur. J. **4**, 2136 (1998). https://doi.org/10.1002/(SICI)1521-3765(19981102)4:11<2136::AID-CHEM2136>3.0.CO;2-G
23. S. K. Wolff, D. J. Grimwood, J. J. McKinnon, M. J. Turner, D. Jayatilaka, M. A. Spackman, Crystal Explorer 3.1 (University of Western Australia, Crawley, Western Australia, 2005–2013). http://hirshfeldsurface.net/CrystalExplorer.
24. M. A. Spackman and D. Jayatilaka, Cryst. Eng. Comm. **11**, 19 (2009). https://doi.org/10.1039/B818330A